

Structural study of a so-called $\text{Mn}^{3+}/\text{Mn}^{4+}$ charge ordered $\text{Pr}_{0.60}\text{Ca}_{0.40}\text{MnO}_3$ single crystal: evidence that electronic localization, occur at a larger scale than the atomic one.

A. Daoud-Aladine,¹ J. Rodríguez-Carvajal,¹ L. Pinsard-Gaudart,^{1,2} M.T. Fernández-Díaz,³ and A. Revcolevschi²

¹Laboratoire Léon Brillouin, CEA-CNRS Saclay, 91191 Gif sur Yvette

²Laboratoire de Physico-Chimie de l'Etat Solide, Université Paris Sud, Bât. 414, 91405 Orsay

³Institut Laue Langevin, 38042 Grenoble

(Dated: December 2, 2024)

In the $\text{R}_{1-x}\text{D}_x\text{MnO}_3$ manganites (R: rare earth, D: divalent cation), the structural phase transition at T_{CO} is commonly interpreted as a concomitant charge and orbital ordering (CO/OO) process driven by a cooperative Jahn-Teller effect and Coulomb repulsion forces. Full crystal structure refinement, from a neutron diffraction experiment below T_{CO} on a $\text{Pr}_{0.60}\text{Ca}_{0.40}\text{MnO}_3$ single crystal, gives us a model for the displacement of atoms with respect to the high temperature (HT) phase that invalidates the standard model based on the CO/OO picture. An alternative picture is that the phase transition and charge localization at T_{CO} arise from a spatially ordered condensation of ferromagnetic Mn-Mn pairs, in which Mn atoms keeps an intermediate valence state.

PACS numbers: 71.27.+a, 71.30.+h, 61.12.-q, 75.10.-b

The calcium-doped manganites $\text{R}_{1/2}\text{Ca}_{1/2}\text{MnO}_3$ ($x \approx 0.5$) (R: rare-earth) are known to display a structural phase transition at T_{CO} attributed to charge and orbital orderings, because it is associated with a jump in the resistivity and to the onset of superstructure reflections in the low temperature (LT) phase with $\mathbf{q} = (0, 1/2, 0)$ in electron, X-ray and neutron diffraction patterns [1, 2]. Moreover, they display another unique signature consisting of a complex AF CE-type spin ordering at a temperature $T_N < T_{CO}$. This can be comprehensively understood using the semi-empirical Goodenough-Kanamori-Anderson (GKA) rules for the superexchange interactions, applied to a model of orbital ordering of the Mn^{3+} d_{z^2} orbitals in the (a,b) plane, proposed in the late fifties by Goodenough [3, 4]. The fact that Goodenough's model (GM) suggests a charge ordered pattern of Mn^{3+} and Mn^{4+} ions in a NaCl-type lattice, has raised the idea that the magneto-transport properties of these

compounds are strongly influenced by dynamic CO/OO driven by the combined effect of Coulomb repulsion and Jahn-Teller distortion around the Mn^{3+} sites [5, 6]. The superstructure is the result of modulated atomic displacements accompanying the electronic localization, but the very nature of the transition should be deduced from the analysis of a detailed structure determination not needing *a priori* constraints. It is expected that CO will result in the setting up of MnO_6 octahedra of different average Mn-O distances (d_{MnO}), as it is empirically well established by the Bond Valence Model (BVM) [7]. Note that in LaMnO_3 and CaMnO_3 , the d_{MnO} are respectively 2.02 Å (Mn^{3+}) and 1.90 Å (Mn^{4+}). A NaCl-like CO without OO is also compatible with a transition characterized by $\mathbf{q}_{CO} = (0, 0, 0)$ in the $Pbnm$ setting, so that several subgroups of $Pbnm$ are possible. This is the case of the charge disproportionation observed in the metal-insulator transition of RNiO_3 (R=Ho, Y, Er, Tm, Yb, and Lu) [8]. A Jahn-Teller driven orbital ordering should also differentiate the octahedra by their distortion. The experimental determination of these displacements has been attempted on several manganites, following the work of Radaelli et al. [6] on $\text{La}_{1/2}\text{Ca}_{1/2}\text{MnO}_3$. The small number of weak superstructure reflections observable by X-ray or neutron powder diffraction makes the published results dubious, since structural models have to be constrained in order to obtain stable refinements [6, 9, 10, 11, 12]. The constraints that have been used are those one would expect from the *a priori* assumption that the GM is the *correct* one. The GM of CO/OO-orbital ordering for $\text{R}_{1/2}\text{D}_{1/2}\text{MnO}_3$ perovskites have only been justified, from powder diffraction experiments, by introducing constraints between the free parameters of the space group $P112_1/m$ that imposes a pattern of atom displacements as depicted in Fig.1a.

By contrast, in LiMn_2O_4 [13], a Mn oxide with a cubic

TABLE I: Octahedral distortions in $\text{Pr}_{0.60}\text{Ca}_{0.40}\text{MnO}_3$. $\Delta = \frac{1}{6} \sum_{i=1}^6 \left| \frac{d_{MnO_i} - \langle d_{MnO} \rangle}{\langle d_{MnO} \rangle} \right|^2$ measure the octahedron regularity. The Bond Valence Sums (BVS), uses the $\text{Mn}^{3+}d_0$ -parameter for all sites (see ref[13] for definitions).

$T = 280K$		$T = 195K$	
Mn site	Mn ₁ site	Mn ₂ site	
Mn-O _{ap} :1.953(1)(×2)	Mn ₁ -O ₁ :1.951(3)	Mn ₂ -O ₃ :1.957(3)	
Mn-O _{eq} :1.967(2)(×2)	Mn ₁ -O ₂ :1.942(3)	Mn ₂ -O ₄ :1.940(3)	
Mn-O _{eq} :1.953(1)(×2)	Mn ₁ -O ₁ :1.879(2)	Mn ₂ -O ₄ :1.899(2)	
	Mn ₁ -O ₁ :2.053(2)	Mn ₂ -O ₄ :2.028(2)	
	Mn ₁ -O ₃ :1.980(2)	Mn ₂ -O ₃ :2.011(2)	
	Mn ₁ -O ₂ :1.955(2)	Mn ₂ -O ₂ :1.899(2)	
$d_{MnO}=1.957(1)$ Å	$d_{MnO}=1.960(1)$ Å	$d_{MnO}=1.955(1)$ Å	
BVS=3.52	BVS=3.53(1)	BVS=3.50(1)	
$\Delta(\times 10^{-4})=0.12$	$\Delta(\times 10^{-4})=6.99$	$\Delta(\times 10^{-4})=6.506$	

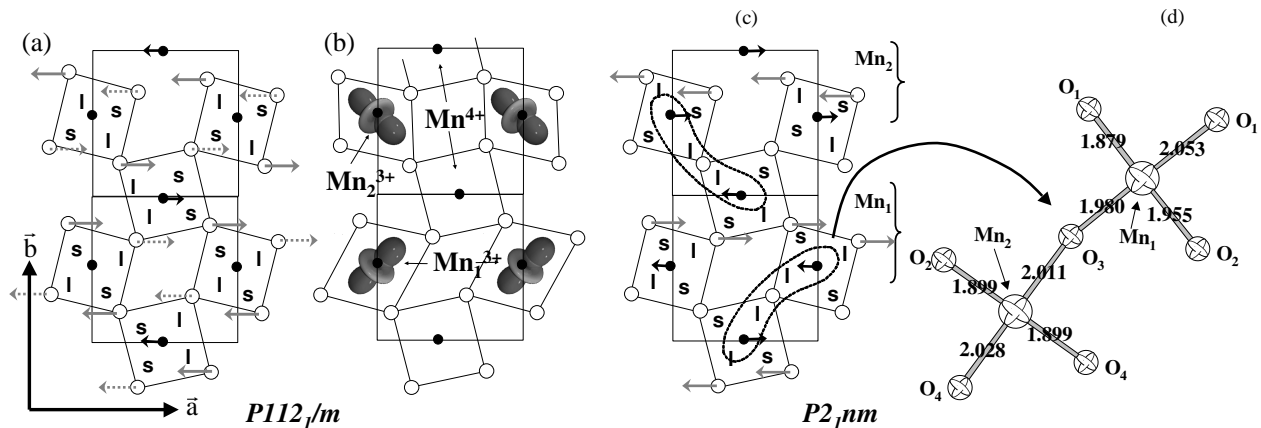


FIG. 1: MnO₂ (a,b) planes of the structure: schematic representation of the displacements of the atoms with respect to their average $Pbnm$ positions, that are exaggerated for clarity, in the $P112_1/m$ symmetry (a) and with $P2_1nm$ symmetry (c) respectively. Labels "l" and "s" are for long (≈ 2 Å) and short (≈ 1.9 Å) Mn-O distances. The refinement of from our single crystal data with the $P112_1/m$ symmetry the gives: for the 827 measured fundamental lines, $R_{F_2}^f$ factor : 4.21% and for 722 superstructure lines, $R_{F_2}^{ss}$ factor : 39.3%. With the $P2_1nm$ symmetry refinements gives $R_{F_2}^f$ factor : 2.62% and $R_{F_2}^{ss}$ factor : 10.8 % (see Fig.2) . (b) is the standard CO/OO model deduced from (a). (d) show the Mn-O distances around one $Mn_1-O_3-Mn_2$ unit, represented by the lobes on the figure (c).

spinel structure, charge ordering, together with a cooperative Jahn-Teller effect, is clearly established below the structural transition around RT. The CO/OO picture is so widely accepted to describe the properties of half doped manganites that the use of the associated jargon hides the today's lack of a non-ambiguous atom displacements pattern properly explaining the intensity of a high number of superstructure reflections. The literature in the field is plenty of assumptions that are not justified from our point of view. The appearance of reflections of type $(0, k, 0)$ with k odd, in $Pbnm$ notation, is automatically attributed to CO and the reflections indexed with the propagation vector $\mathbf{q} = (0, 1/2, 0)$, $(h, k + \frac{1}{2}, l)$, to OO. The appearance of these reflections are just due to a structural phase transition, the origin of the phase transition may be other than CO/OO. The literature concerning resonant x-ray scattering (RIXS) is particularly prone to these misunderstandings [14, 15], due to the fact that the interpretation of the experimental outcomes is still controversial [16, 17].

In this Letter, we report a complete structure refinement of a $Pr_{0.60}Ca_{0.40}MnO_3$ single crystal. We selected the Pr-Ca system for two reasons: (1) it is an archetype of the so called CO-manganites, in which the CO-phase is known to be stable down to the $x = 0.3$ doping level [2, 11, 18]; (2) the similar ionic radius of Pr^{3+} and Ca^{2+} makes the size mismatch effects negligible, minimizing the differences between the average displacements, observed by analyzing the Bragg reflections, and the local oxygen displacement induced by chemical disorder. The data collection was performed using the 2D detector of the four circle diffractometer D9 at the Institute Laue-

Langevin in Grenoble. The study of the magnetic structure, at $T = 15K$ ($T_N = 170K$) gives a canted AF-CE structure with an angle between the moment direction and the \mathbf{c} -axis equal to $\theta = 28^\circ$, consistent with the dependence of θ as a function of the composition found in the literature. The characterization of a crushed piece of the same crystal using synchrotron high resolution powder diffraction (SHRPD), confirms the crystal is greatly homogeneous since it displays a single phase pattern at $T = 250K$ above $T_{CO} = 240K$. Its stoichiometry, refined by combined refinements of single crystal neutron diffraction and synchrotron data is $x = 0.40(1)$. Complementary XANES experiments have also been carried out in other powder samples of similar compositions. A complete description of all our synchrotron results, including the defect microstructure, as well as the technical details of the neutron diffraction refinements is out of the scope of this Letter, and will be published elsewhere.

The problem of structure refinement of the neutron diffraction data in these orthorhombic perovskites arises from the intrinsic twinning of the crystals. Here, it can be solved thanks to the small distortion $Pr_{0.60}Ca_{0.40}MnO_3$ present at all temperatures. A single integrated intensity has contributions from different domains. This can be handled by the program FULLPROF [19] that allows us to refine a common structural model by adding the contribution of all domains. At $T = 280K$, 416 reflections were used for the refinements, and the R_{F_2} factor is 3.03%. The structure is orthorhombic with $Pbnm$ symmetry, very similar to the already published data [2]. Its cell parameters (SXHRDP data) are $a = 5.4210(1)\text{Å}$, $b = 5.4460(1)\text{Å}$ and $c = 7.6480(1)\text{Å}$. It has a unique Mn

site and displays a pattern made of tilted nearly regular octahedra, whose d_{MnO} is characteristic of an intermediate valence site (see table I).

Below T_{CO} at $T = 195K$, the most intense superstructure peaks are found to have 2.7% of the intensity of the most intense fundamental peaks. Group theory gives six isotropy subgroups of $Pbnm$ having a doubled cell along \mathbf{b} , among which we have performed unconstrained refinements, except for symmetry. Any one of the three isotropy subgroups keeping the m mirror plane perpendicular to the \mathbf{c} direction of the HT phase, gives rather good results fits to the fundamental reflections. But the intensity of superstructure lines are much better described by the space groups $P2_1nm$ or $P11m$ than by the group $P112_1/m$ which, we recall, was the previously reported candidate for the symmetry of the CO phase (see Fig. 2 and caption of Fig.1 for the reliability factors). Note that $P11m$ being a subgroup of both $P112_1/m$ and $P2_1nm$, it could allow to describe displacements as expected from the GM. Our study demonstrates that the experimentally refined displacement model with $P11m$ symmetry gives a strong $P2_1nm$ pseudo-symmetry. Indeed, the refined atomic positions give no significant differences using either $P2_1nm$ or $P11m$ models, except that the number, and therefore the correlations, of the parameters in $P11m$ are greater. Hence, the true space group is $P11m$, since we know from the SHRPD study, that the metric is monoclinic, but the refined structural parameters can be described in the $P2_1nm$ group. They are given in Table II and a schematic pattern of the atomic displacements is displayed in Fig.1c. When we compare them to those of Fig.1a, we see that in both cases, the displacements are mainly along the \mathbf{a} -axis. The symmetry imposed inversion center on the Mn sites identified to Mn^{3+} in the $P112_1/m$ description allow only symmetric oxygen displacement around these Mn. This symmetry imposed constraint is lifted in the non-centrosymmetric group $P2_1nm$ (Fig. 1c). This allow all the Mn ions in the structure to move off center in their slightly elongated MnO_6 octahedron which keep otherwise almost regular local orthogonal axes (Fig. 1c). All these structural details are inconsistent with the ionic picture of concomitant Mn^{3+}/Mn^{4+} CO and d_{z^2} OO. In particular the persistence of an intermediate valence state for the Mn atoms in the LT phase is confirmed by the very similar d_{MnO} on the two sites (see Table I).

The XANES study of the Mn valence state using the Mn K-edge we performed on a $Pr_{1-x}Ca_xMnO_3$ ($x = 1/2$) powder sample lead to the same conclusion as the analysis recently published by Garcia et al. [20]. The sample presents, at all temperatures, a spectra that have a sharp slope at the edge. This contradicts the CO picture for the LT phase, where for a mixing of localized Mn^{3+} and Mn^{4+} electronic states, the spectrum is expected to be linear combination of the end members $RMnO_3$ and $DMnO_3$ XANES spectra, resulting in a broad shape and

TABLE II: Refinement of structural parameters of $Pr_{0.60}Ca_{0.40}MnO_3$ at $T=195K$ in the orthorhombic $P2_1nm$ pseudo-symmetry, the real structure is monoclinic $P11m$ with cell parameters $a = 5.4315(1)\text{\AA}$, $b = 10.8970(2)\text{\AA}$, $c = 7.6370(1)\text{\AA}$, $\gamma = 90.076(2)^\circ$. The doubled cell origin is shifted by a $(0\ 3/4\ 1/4)$ translation with respect to the high temperature orthorhombic $Pbnm$ phase.

Atom	Wyck. Pos.	x	y	z	B_{iso} (\AA^2)
Pr/Ca ₁	2a	0.5121(4)	0.8936(2)	0	0.53(3)
Pr/Ca ₂	2a	0.4784(4)	0.3614(2)	1/2	0.77(3)
Pr/Ca ₃	4b	-0.0023(4)	0.1426(2)	0	0.56(3)
Pr/Ca ₄	4b	0.9905(4)	0.6088(2)	1/2	0.25(2)
Mn ₁	2a	0	0.8756(2)	0.2489(3)	0.31(2)
Mn ₂	2a	0.9795(2)	0.3746(1)	0.7492(4)	0.13(2)
O ₁	4b	0.3044(4)	0.9845(1)	0.2861(2)	0.26(2)
O ₂	4b	0.7090(4)	0.2676(1)	0.7891(2)	0.48(1)
O ₃	4b	0.2112(4)	0.2328(1)	0.7148(2)	0.96(2)
O ₄	4b	0.7515(4)	0.5191(1)	0.2110(2)	0.41(2)
O' ₁	2a	0.4353(4)	0.1125(2)	0	0.41(2)
O' ₂	2a	0.5743(4)	0.1321(2)	1/2	0.68(3)
O' ₃	2a	0.0562(4)	0.3758(1)	0	0.33(2)
O' ₄	2a	0.9104(4)	0.3846(2)	1/2	0.69(2)

a pronounced structure. However, the octahedral distortions below T_{CO} manifest themselves as small changes that are located at energies well above the edge. They reduce also the pre-peak intensity, which can be interpreted as hole ordering on oxygen sites together with an increase in the covalency of Mn $3d$ and O $2p$ states rather than Mn^{3+}/Mn^{4+} charge ordering [21]. The off-centering of Mn atom in our structural model also make the dipole $1s - 3d$ transitions allowed via $3d - 4p$ mixing on the absorbing site, which had never been seriously considered since Mn sites have always been considered as centrosymmetric insofar [22]. At last, this distortion leads also to an anisotropy of the anomalous scattering factor, that may be sufficient to observe resonant "forbidden" reflections with the RIXS technique [17], which are not necessarily

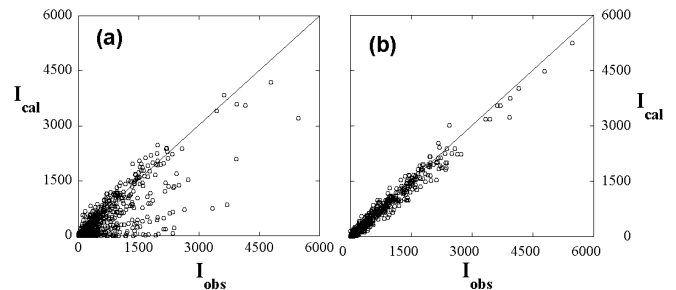


FIG. 2: Observed vs calculated intensity of superstructure lines indexed as $(h, k + 1/2, l)$ in the HT cell setting, in $Pr_{0.60}Ca_{0.40}MnO_3$ with $P112_1/m$ (a) and $P2_1nm$ (b) structural models.

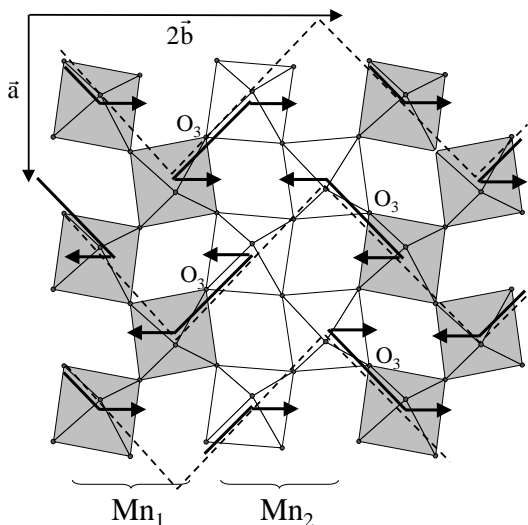


FIG. 3: Dashed line represent the zig-zag chains of the ferromagnetically coupled spins. The O₃ equatorial oxygen are shown.

associated here, to different charge densities around the Mn atoms. Therefore, this show that the apparent contradiction [14, 20] of the XANES and RIXS techniques can be re-interpreted in view of the particular distortion pattern we find.

The structure geometry at LT display elongated octahedra in the Mn₁-O₃-Mn₂ direction. To understand the covalency increase together with an electronic localization process below T_{CO} evidenced by resistivity measurements, one should imagine this increase arises within the Mn₁-O₃-Mn₂ units, where one electron is shared (delocalized) leading to mixed localized states of $d_{z^2} - 2p_{\sigma} - d_{z^2}$ character. This is consistent with the Mn₁-O₃-Mn₂ angle becoming the most opened angle (161°), suggesting further this electron delocalization is favored by tuning on a local double exchange (DE) process within each Mn₁-Mn₂ pair, maintaining the intermediate valence of both Mn atoms in the ionic picture. In other words, this interpretation of the structural distortions emphasizes the appearance, just below T_{CO} , of ordered Mn₁-O₃-Mn₂ molecular objects with ferromagnetically coupled Mn moments. The hypothesis of the existence of such ferromagnetic coupled Mn-pairs gives also a clue to interpret the anomaly in the magnetic susceptibility observed at the supposedly purely structural transition [23, 24], for samples that remain in a paramagnetic state below T_{CO} . Their formation should lead to new elemental paramagnetic units with a higher effective moment. This seems to be confirmed by the increase of the Curie constant $C = \frac{N\mu_{eff}^2}{k_B}$ in the region between T_{CO} and T_N in Bi_{1/2}Sr_{1/2}MnO₃, where there is no magnetic contribution arising from the paramagnetic rare-earth element [25]. The non validity of the ionic picture changes also our understanding of the CE-type magnetic structure.

We think that the GKA rules for the super exchange interaction cannot be totally applied to the present case because the system preserves an itinerant nature even if it is at the level of structural dimers. One should note that the Mn₁-Mn₂ ferromagnetically coupled pairs are linked into zigzag chains, which are the building blocks of the CE structure, as displayed in Fig.3. Below T_N , AF superexchange coupling can occur between these molecular objects with localized electronic states. They should be mediated by the non-labeled oxygen atoms of the Fig. 3 to stabilize the observed CE structure.

In conclusion, the present study invalidates the widely used ionic picture of charge ordering invoked to interpret the jump of the resistivity and the appearance of superstructure reflections at the structural transition in the Pr_{1-x}Ca_xMnO₃ system. The results presented in this Letter favor a description in term of an anisotropic charge redistribution different from the CO/OO model proposed by Goodenough. The transition may be interpreted in terms of the condensation and ordering of ferromagnetic Mn-Mn pairs remaining paramagnetic below T_{CO} and giving rise, below T_N , to different variants of the CE magnetic structure depending on the exact stoichiometry.

We would like to thank P.Berthet, for his help in carrying out the XANES experiments at LURE (ORSAY, France).

-
- [1] S. Mori *et al.*, Nature **392**, 473 (1998).
 - [2] Z. Jirak *et al.*, J. Magn. Magn. Mat. **53**, 153 (1985).
 - [3] J. B. Goodenough, Phys. Rev. **100**, 564 (1955).
 - [4] E. O. Wollan *et al.*, Phys. Rev. **100**, 545 (1955).
 - [5] C. Chen *et al.*, Phys. Rev. Lett. **83**, 4792 (1999).
 - [6] P. Radaelli *et al.*, Phys. Rev. B **55**, 3015 (1997).
 - [7] I. Brown, Acta Cryst. **B48**, 553 (1992).
 - [8] J. Alonso *et al.*, Phys. Rev. B **61**, 1756 (2000).
 - [9] J. Blasco *et al.*, J. Phys.: Cond. Matt. **9**, 10321 (1997).
 - [10] P. M. Woodward *et al.*, Chem. Mat. **11**, 3528 (1999).
 - [11] Z. Jirak *et al.*, Phys. Rev. B **61**, 1181 (2000).
 - [12] O. Richard *et al.*, Acta Cryst. **A55**, 704 (1999).
 - [13] J. Rodriguez-Carvajal *et al.*, Phys. Rev. Lett. **81**, 4660 (1998).
 - [14] M. v. Zimmermann *et al.*, Phys. Rev. Lett. **83**, 4872 (1999).
 - [15] Y. Wakabayashi *et al.*, J. of Phys. Soc. Jap. **69**, 2731 (2000).
 - [16] Y. Joly *et al.*, AIP Conf. Proc. **514**, 30 (2000).
 - [17] J. Garcia *et al.*, J. Phys.: Cond. Matt. **13**, 3243 (2001).
 - [18] Y. Tokura *et al.*, J. Magn. Magn. Mat. **200**, 1 (1999).
 - [19] J. Rodriguez-Carvajal, Physica-B **192**, 55 (1993), <http://www.ccp14.ac.uk/tutorial/fullprof/>.
 - [20] J. Garcia *et al.*, J. Phys.: Cond. Matt. **13**, 3229 (2001).
 - [21] A. Y. Ignatov *et al.*, Phys. Rev. B **64**, 014413 (2001).
 - [22] F. Bridges *et al.*, Phys. Rev. B **63**, 214405 (2001).
 - [23] F. Millange *et al.*, Phys. Rev. B **62**, 5619 (2000).
 - [24] M. Lees *et al.*, Phys. Rev. B **52**, 14303 (1995).
 - [25] J. L. García-Muñoz *et al.*, Phys. Rev. B **63**, 064415

(2001).